Size and Surface Chemistry Tuning of Silicon Carbide Nanoparticles

Sergei Alekseev[a,b*], Elena Shamatulskaya[a], Mykola Volvach[a], Svitlana Gryn[a,b], Dmytro Korytko[a,b], Igor Bezverkhyy[c], Viacheslav Iablokov[d], Vladimir Lysenko[e].

[a] *Taras Shevchenko National University of Kyiv, 62a, Volodymyrs'ka Street, 01601 Kyiv, Ukraine*

[b] *Science Park Kyiv Taras Shevchenko University, 60, Volodymyrs'ka Street, 01033 Kyiv, Ukraine*

[c] *Laboratoire Interdisciplinaire Carnot de Bourgogne, UMR CNRS 6303, Universite de Bourgogne, France*

[d] *Voiland School of Chemical Engineering and Bioengineering, Washington State University, Pullman, Washington 99164, USA.*

[e] *University of Lyon, Nanotechnology Institute of Lyon (INL), UMR CNRS 5270, INSA de Lyon, France*

[*] Contact author, e-mail : *alekseev@univ.kiev.ua*

TOC Graphic

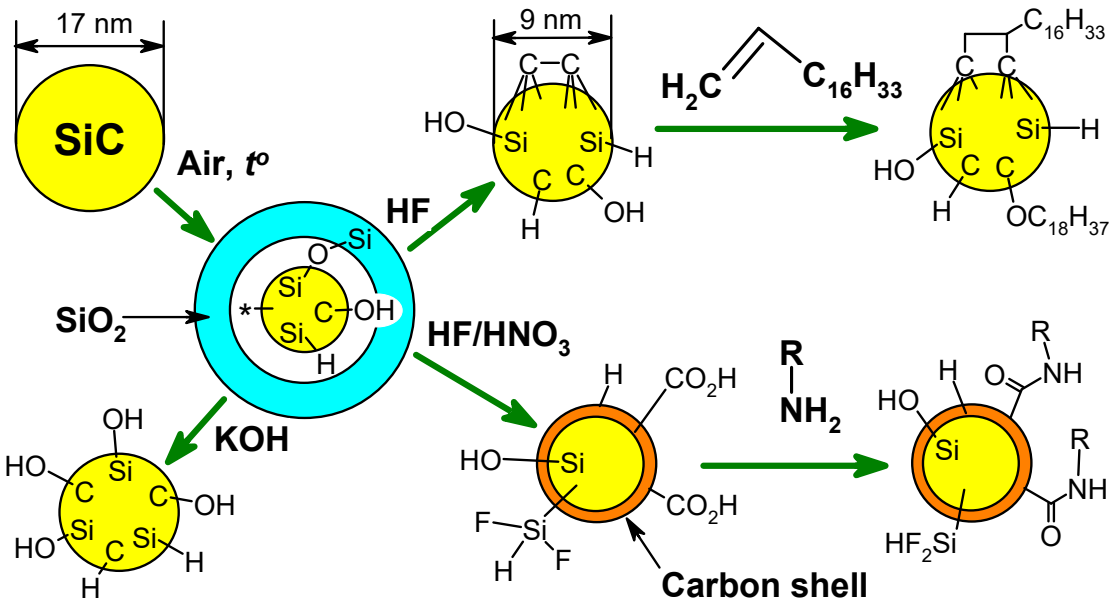

Abstract

Chemical transformations on the surface of commercially available 3C-SiC nanoparticles were studied by means of FTIR, XPS and temperature-programmed desorption mass spectrometry methods. Thermal oxidation of SiC NPs resulted in the formation of a hydroxylated SiO_2 surface layer with $C_3Si–H$ and CH_x groups over the SiO_2/SiC interface. Controllable oxidation followed by oxide dissolution in HF or KOH solution allowed the SiC NPs size tuning from 17 to 9 nm. Oxide-free SiC surfaces, terminated by hydroxyls and $C_3Si–H$ groups, can be efficiently functionalized by alkenes under thermal or photochemical initiation. Treatment of SiC NPs by HF/HNO_3 mixture produces a carbon-enriched surface layer with carboxylic acid groups susceptible to amide chemistry functionalization. The hydroxylated, carboxylated and aminated SiC NPs form stable aqueous sols.

1. Introduction

Among the vast variety of currently known inorganic materials, the silicon carbide (SiC) exhibits a number of unique properties [1]. The SiC possesses outstanding thermal conductivity [2]; thermal, mechanical and chemical stability, which results in low toxicity and biocompatibility. It is a wide band-gap semiconductor (ΔE = 2.36 eV for 3C-SiC polytype) giving optical effects such as visible range photoluminescence [3, 4], electroluminescence (the first LED was built on SiC [5]) and second harmonic generation [6, 7]. That is why SiC-based nanostructures such as porous SiC [8, 9], SiC nanowires [10, 11] and particles attract growing attention of scientific community. In particular, the SiC nanoparticles (NPs) can be applied in microelectronics, as initial materials for ceramics [12] and composites [13, 14, 15], as abrasives, catalyst support [16], photocatalysts [17, 18, 19], biosensors [20], adsorbents [21, 22] and in biology as optical probes [23, 24, 25].

Variable properties of the SiC NPs, such as sintering, dispersibility in liquids and polymers, stability, viscosity and electrokinetical properties of aqueous sols, optical and biological properties are all determined mainly by the composition of the NPs surface layer and can be tuned by appropriate chemical modification. The size of SiC NPs also matters on their properties. That is why the surface chemistry of the SiC is a research focus of numerous researchers.

Different protocols used for the preparation of SiC nanostructures led to a wide variety of SiC surface terminations, which are characterized sufficiently well. However, the diversity of “initial” SiC surface chemistries makes further chemical functionalization of the SiC surface complicated and poorly studied problem. Furthermore, three different types of SiC materials under study, i.e.: i) monocrystalline wafers; ii) the SiC nanostructures prepared by partial chemical or electrochemical dissolution of bulk SiC, referenced below as “top-down nano-SiC”, and iii) “industry-made SiC powders” form three practically independent data clusters; that “separation” occurs probably due to difference in the applied methods and interest fields of researchers dealing with those materials. As a

result of all aforementioned, many aspects related to the chemical properties of the SiC surface remain unexplored and poorly studied in comparison with other semiconductors.

Large arrays of data concerning the surfaces of SiC monocrystals have been mainly obtained with the help of XPS and multiple reflection FTIR-ATR methods. Particularly, treatment of both "carbon" and "silicon" faces of the oxidized 4H-SiC plate with HF resulted in formation of highly hydrophilic surfaces, bearing mainly hydroxyl groups (≡C–OH and ≡Si–OH) respectively [26]. According to Rosso *et al.* [27, 28], HF-treated surfaces of the SiC readily react with alkenes under thermal or photochemical activation leading to hydrolytically stable grafted layers due to formation of C–O–C bridges between the ≡C–OH groups and alkene molecules. Easily polymerizable alkenes, such as styrene and methacrylates, form polymer brushes onto the ≡C–OH groups of the 6H-SiC carbon face under photoinitiation, while ≡Si–OH groups of the silicon face remain inactive under identical conditions [29]. One of the most interesting features of the SiC surface is the reaction of 3C-SiC (100) 3×2 reconstructed surface with hydrogen [30, 31] giving a "metalized" surface. That surface is covered with ≡Si–H bonds and high fraction of sterically stabilized dangling bonds. Besides that, heating of the SiC in high vacuum results in partial evaporation of Si atoms forming a well-structured graphene monolayer on the silicon face of the crystal [32]; in fact, it was the first method of graphene preparation.

Highly-crystalline small ($d < 6.5$ nm) photoluminescent "top-down" SiC NPs can be produced by partial oxidation and dissolution of bulk SiC in HF-based solutions followed by mechanical or ultrasonic grinding of resultant powders. Widely used chemical oxidation of SiC micropowders requires rather harsh fabrication conditions (HNO_3:HF (1:3, v/v) at 100^{o}C) [33, 34, 35, 36, 37], while an electrochemical etching of SiC wafers can be carried out in more controllable way [23, 24, 38, 39]. Recently, the electrochemical procedure was successfully applied to obtain small (< 10 nm) SiC NPs from the slurry of relatively large SiC nanopowder (> 50 nm) [40].

According to different groups of authors [34, 35, 36, 38, 39], the surface of as-prepared "top-down" SiC NPs can be terminated with a wide variety of functionalities, such as hydroxyls, Si–O–Si, Si–O–C and C–O–C bridges, CH_x groups, "sp^2-carbon", silane (Si–H) groups, Si–Si bonds and some fluorine-containing species. The hydroxyls (≡C–OH and ≡Si–OH) as well as carboxylic acid (–CO_2H) groups seems the most well-confirmed among them, demonstrating the acidity constants (pK_a) equal to 4.2 (–CO_2H), 7.1 (≡Si–OH) and 9.5 (≡C–OH) [41]. In general, the surface chemistries of the SiC NPs, prepared by either chemical or electrochemical dissolution, are similar between themselves and to those of electrochemically-derived porous 6H-SiC [42]. Additionally it should be mentioned, that oxidation of the SiC in HF-containing solutions may result in the formation of a by-product named carbon fluorooxide [43], the presence of which could influence the interpretation of SiC chemical, photoluminescent and biological properties.

Commercially available SiC NPs are usually prepared by "bottom-up" methods, such as carbothermal reduction [9, 44] or plasmochemical and CVD processes [1, 45]. Resultant NPs usually possess higher concentration of crystallite defects, larger particle size and completely different initial surface termination in comparison with the "top-down" nano-SiC. For example, detailed XPS and elemental analysis studies were carried over industry-made by CVD 30-50 nm SiC nanopowders. It was shown that the presence of carbon, silicon oxide (SiO_2) or oxocarbide (SiOC) surface species varied with the preparation conditions [46].

Chemical functionalization of the SiC is commonly performed through the hydroxyl groups via the silanization route, well developed for the surface of SiO_2. That procedure was successfully applied for monocrystalline SiC [47, 48], industry-made SiC NPs [49, 50, 51] and thermally-oxidized porous SiC [42]. Another efficient method of modification and control of colloidal properties of the SiC NPs is a non-covalent bonding of soluble polymers [52, 53]. Hydrolytically stable grafted layers could be formed on the SiC NPs by thermal decomposition of azo initiators [54], via the interaction of free radicals with unsaturated carbon bonds of SiC surface according to authors' suggestion. The

carboxylic acid groups on the “top-down” nano-SiC are able to form salts, anhydrides, amides etc., making them a prospect for further functionalization [41, 42, 55].

In the present work, we attempted to study several issues limiting practical applications of commercially available SiC nanopowders in nanoscience. The size of well-crystalline industry-made SiC particles is commonly large (above 15-20 nm according to manufacturer’s specifications) in comparison with the “top-down” SiC NPs. Their surface chemistry is uncertain due to variations in preparation methods and post-production history. All of this limits the possibility of SiC NPs chemical functionalization, preparation of their stable sols, their application for bioimaging, and etc. Herein, we propose a relatively simple procedure of the SiC NPs size tuning, protocols of simplification of their surface chemistry, procedures of chemical functionalization of oxide-free NPs as well as preparation of their stable aqueous sols without additional stabilizing agents.

2. Experimental Section

2.1. Chemical transformations of SiC nanoparticles

Initial SiC nanoparticles (SiC_init) were purchased from Nanostructured & Amorphous Materials, Inc. (NanoAmor, USA). According to suppliers data this material contains 97% of beta SiC (3C-SiC) having 10-20 nm particle size and 150-200 $m^2 \cdot g^{-1}$ surface area. The NPs looked like a black highly dispersed powder with very low (0.08 $g \cdot cm^{-3}$) bulk density.

Thermal oxidation of SiC NPs was performed by means of their annealing in air with a ramp of 10 $^oC \cdot min^{-1}$ afterwards the temperature was kept for 1 hour at the desired value (from 400 to 900 ^oC). The samples of this series are referenced as SiC_900 (for example).

Acidic removal of surface oxide was performed by treatment of oxidized SiC NPs with HF (48%) and ethanol mixture (1:9, v/v) for 15 minutes. Treated SiC NPs were settled by centrifugation (any centrifugation was performed for 15 minutes at 14000 g unless otherwise is specified), washed under centrifugation repeatedly with water and afterwards with 0.01 M HCl (to suppress peptization),

then dried at 70°C in air. The samples of this series are referenced as SiC_900_HF (for example). Alkaline removal of the oxide layer was performed by SiC NPs treatment with oxygen-free 5M KOH for 30 min followed by washing and drying (optionally) according to above protocol.

To perform SiC NPs surface oxidation in the conditions, avoiding formation of oxide layer, the sample SiC_600 was treated with HF (48%):HNO_3 (70%) mixture (9:1, v/v) at 100°C for 15 min to obtain SiC_HF/HNO_3 sample. For characterization and further modifications this sample was washed according to the same protocol, as the samples of SiC_t°C_HF series. For pH titration and zeta-potential measurements the sample SiC_HF/HNO_3 after preliminary acids removal was additionally kept in 0.1 M KOH to ensure hydrolysis of Si–F fragments, followed by H_2O and 0.01 M HCl washing steps.

Chemical functionalization of SiC_600_HF with octadecyl groups was performed by 1-octadecene in N_2 atmosphere under thermochemical activation (130°C, 6 h) to get SiC–C_{18}(t) sample or photochemical activation (235 nm, 2 h) to get SiC–C_{18}(hν) sample. Then the SiC–C_{18} NPs were consequently washed with hexane and ethanol under centrifugation.

Reaction of the SiC_HF/HNO_3 with $C_9H_{19}NH_2$ to obtain SiC–NHC_9 sample was performed by refluxing of the particles in 20% solution of $C_9H_{19}NH_2$ in o-xylene for 1 hour. Then the NPs were consequently washed with hexane, ethanol, 3% ethanolic HCl and ethanol under centrifugation. Aminated SiC NPs were prepared by reaction of the SiC_HF/HNO_3 with ethylenediamine (20%) in glycerol at 120°C under continuous mix for 1 hour. The reaction mixture was diluted by ethanol; the particles (SiC_NH_2) were centrifuged down and washed several times with ethanol.

Drying of any powder samples was performed in air at temperature not exceeding 70°C. To prepare aqueous sols of SiC_KOH, SiC_HF/HNO_3 and SiC_NH_2 NPs their suspensions just after the syntheses were washed twice with H_2O under centrifugation to remove excess of electrolytes. The precipitates were diluted with H_2O to obtain 0.05 mg·ml^{-1} concentration in regard to initial powder. The pellets peptize easily under shaking; the resulted suspensions were additionally vortexed and

treated for 30 min in Elmasonic P 30H ultrasonic bath. Large particles (if any present) were removed by 5 min centrifugation at 1500 g. Resulted sols are yellow-brownish transparent liquids, colloidally stable under storage in close vessels for at least 1 year.

2.2. Characterization Methods

X-ray diffraction patterns were recorded on a Shimadzu XRD 6000 diffractometer (CuK_α, 2θ = 5 – 80 deg., 1 deg·min^{-1} scan rate). The size of the ordered (crystalline) domains was estimated by a simple Scherrer formula [56].

Transmission electron microscopy (TEM) observations were performed using a JEOL JEM-2100 microscope at an acceleration voltage of 200 kV. Samples were prepared by deposition from a suspension in ethanol on a carbon-covered copper grid. The particle size distributions were determined using free ImageJ software.

The nitrogen adsorption/desorption isotherms were measured on an ASAP 2020 Micromeritics instrument at 77 K and treated using standard ASAP software. BET method was applied to determine specific surface areas (S_{BET}), while no micropores, the presence of which may strongly affect S_{BET} values, were found by *t*-plot method. The average particle size was calculated from S_{BET} using spherical particle model and average SiC density (3.21 g·cm^{-1}). The relative uncertainty of the values of S_{BET} and calculated average particle sizes is 5%.

FTIR spectra were collected in ambient conditions on a Nicolet Nexus 470 spectrometer in 400 – 4000 cm^{-1} range in transmittance mode (pellets with KBr) or in diffuse reflectance mode using Al mirror as a background.

X-ray photoelectron spectroscopy (XPS) measurements were performed in a combined ToF-SIMS/XPS/STM apparatus at a base pressure of $5 \cdot 10^{-10}$ mbar using non-monochromatic Al K_α-radiation with a power of 130 W. The spectra were recorded for powder samples pressed onto the surface of a gold foil. After subtraction of the Shirley-type background, the core-level spectra were

decomposed into components with mixed Gaussian–Lorentzian (G/L) lines using a non-linear least-squares curve-fitting procedure. The first component of the carbon C 1s peak deconvolution was set at 282.5 eV (standard value for the SiC) and used as reference energy for charge correction. The Si 2p peaks in the final deconvolution are presented as the doublet components sums (Si $2p_{1/2}$ and $2p_{3/2}$ components separated by 0.61 eV with an area ratio equal to 1:2). The Si 2p peaks, presented on the graphs and the peak positions in discussion relate to the sums of the doublets components, otherwise the FWHM values relate to the component itself. The relative uncertainty of the values of surface concentrations of the elements determined from XPS is about 10%.

Temperature programmed desorption mass spectrometry (TPD-MS) measurements were carried out by heating of a dry sample under high vacuum ($p<10^{-3}$ Pa) at a heating rate of 10 $^{o}C \cdot min^{-1}$. The evolving products were analyzed by mass-spectrometry (EI, -70 eV) on a MX7304A instrument (Selmi, Ukraine) [57].

Thermal analysis was performed on a Shimadzu simultaneous TGA/DTA analyser DTG-60H in air at atmospheric pressure with Al_2O_3 as a reference material, heating rate of 10 $^{o}C \cdot min^{-1}$ and 1200 ^{o}C maximum temperature.

Zeta-potentials and dynamic light scattering (DLS) size-distributions were measured by Zetasizer Nano ZS (Malvern) instrument at 173^{o} backscatter geometry for 0.05 $mg \cdot ml^{-1}$ solutions of the NPs, the refractive index of the NPs was taken as 2.65. The relative uncertainty of these measurements is about 10%.

The pH-potentiometric titration by 0.05 M NaOH was performed in 0.05 M NaCl solution, where the sample of SiC NPs was equilibrated for 2 hours prior to titration. All the solutions were prepared on the CO_2-free DI water and an access of CO_2 was minimized during titration.

3. Results and discussion

3.1. Thermal oxidation and size tuning of the SiC nanoparticles

Prior to any treatments, initial SiC NPs were characterized by powder X-ray diffraction (XRD) and TEM. Intense peaks at 35.68, 60.00 and 71.69 deg on the XRD pattern of the NPs (Fig. 1A) correspond to (111), (220) and (311) planes of 3C-SiC, respectively (Joint Committee on Powder Diffraction Standards (JCPDS) card number 29-1129). These peaks are noticeably widened in comparison with the peaks of well-crystallized SiC; the size of ordered (crystallite) domain calculated by a simple Scherrer model from the XRD peak width corresponds to 6.5 nm. Weak XRD peaks at 41.5 and 75.6 deg relate to 3C-SiC planes (002) and (222), while a wide peak centered at 18.2 deg indicates the presence of some amorphous phases such as carbon or SiC_{1+x}.

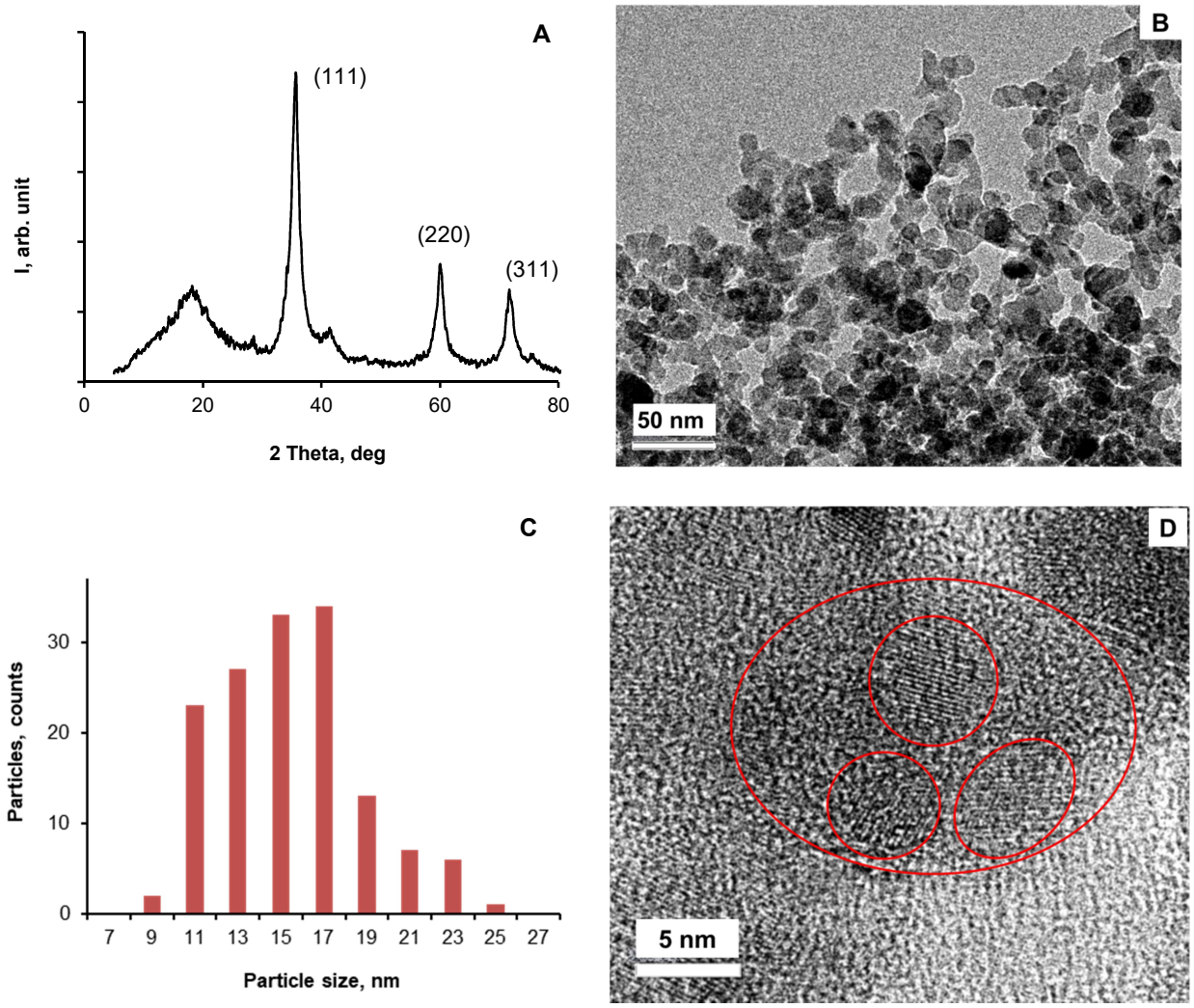

Figure 1. Characterization of initial SiC NPs. A. Powder XRD pattern. B. TEM image. C. Particle size distribution. D. High magnification TEM image.

Additional evidence of the impurities is a black color and typical carbon bands in the Raman spectrum (See Fig. S1, Supplementary Information) of initial SiC NPs. The band gap of 3C-SiC is 2.36 eV wide (525 nm wavelength), so the black color could be caused by carbon, SiC_{1+x} or defects/impurities within SiC lattice.

According to TEM image (Fig. 1B), the sample is composed of irregularly shaped aggregated particles with relatively wide size distribution (Fig. 1C). The mean diameter of the particles from this distribution is equal to 15.5 nm with estimated 3.3 nm standard deviation; the median diameter is 15.3 nm, while a mean mass diameter corresponds to 16.1 nm. High magnification TEM (Fig. 4D) demonstrates atomic planes spaced at 0.25 nm (d_{111} of 3C-SiC). A few crystallites of ~ 5 nm can be distinguished within the particle, which is in a good accordance with the calculation of the crystallite size based on Scherrer model.

The surface area (S_{BET}) of the initial sample, evaluated from nitrogen adsorption isotherm (see Fig. S2, SI) is equal to 110 $m^2 \cdot g^{-1}$. Assuming spherical shape of the SiC particles, their mean size can be estimated as 17 nm ($D = 6 \cdot \rho^{-1} \cdot S^{-1}$; ρ = 3.21 $g \cdot cm^{-1}$ is the density of SiC), which is in perfect accordance with TEM data. All characterization results allow us to state that the initial powder is composed of polycrystalline 3C-SiC NPs with some amorphous impurities and the largest size in the range declared by the manufacturer.

Thermal oxidation resulted in substantial lightening of the SiC NPs color with temperature growth (Fig 2A), which could be seen quantitatively in diffuse reflectance UV-vis spectra (Fig. S3, SI). This change takes place due to removal of black colored carbon and SiC_{1+x} admixtures from the sample under oxidation. Progress of SiC oxidation could be monitored by transmittance FTIR spectra (Fig. 2B). The intensity ratio of the bands at 825 cm^{-1} (TO and LO phonons of SiC lattice) and 1080 cm^{-1} (silicon oxide ν_{as}(Si–O) band) constantly increases with temperature, indicating growth of the oxide layer thickness. The oxide could be seen in TEM images as an amorphous layer on the surface

of SiC NPs (Fig. 2C). Treatment with HF resulted in oxide layer dissolution, which can be observed by vanishing of ν(Si–O) bands in FTIR (Fig. 2B) and amorphous layer in TEM (Fig. 2D).

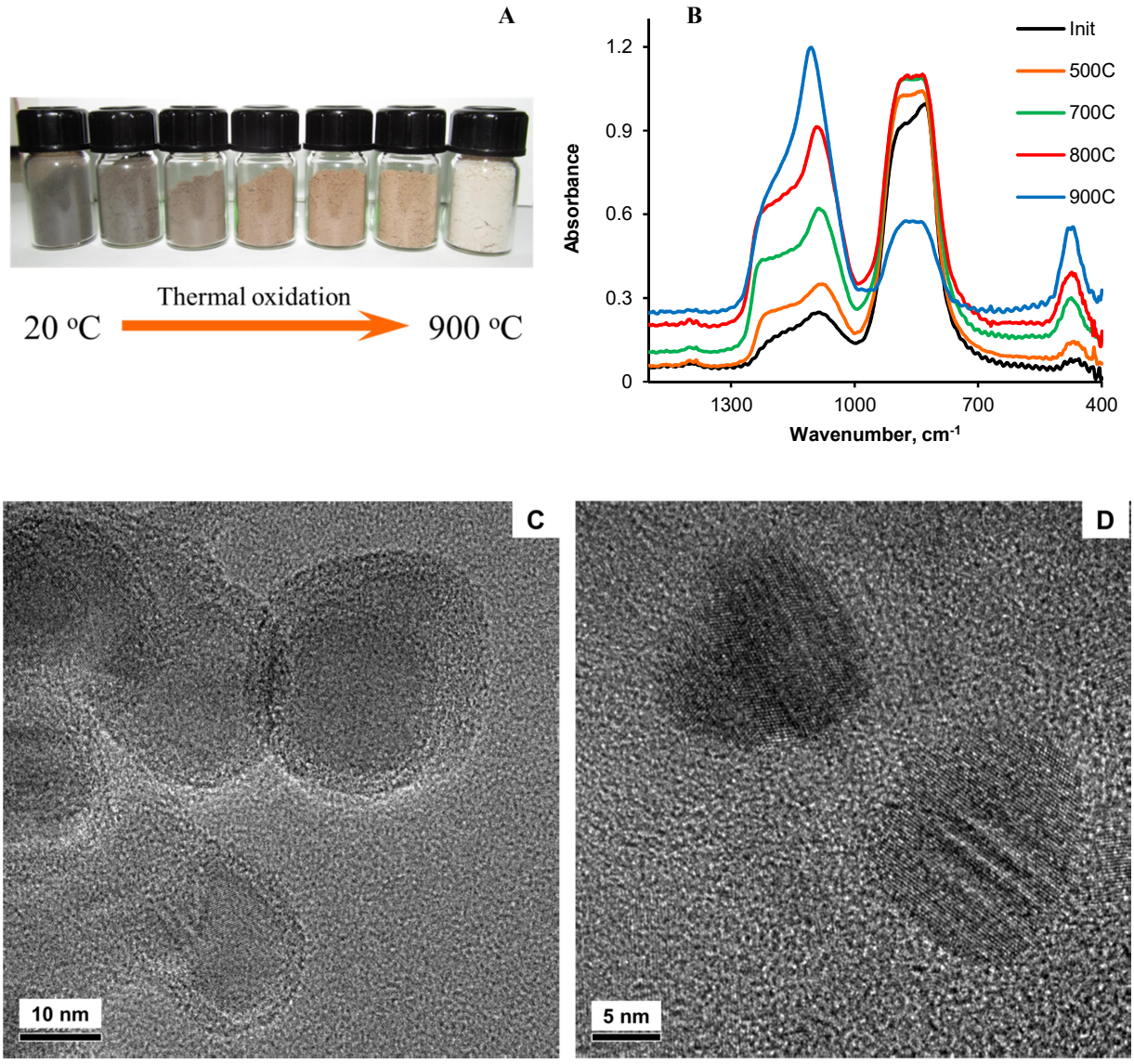

Figure 2. SiC NPs oxidized at different temperatures. A. Optical photos. B. FTIR spectra (KBr pellets). C. TEM image (SiC_900°C). D. TEM image (SiC_900°C_HF): absence of surface oxide layer allowed to obtain more clear image of crystalline planes and dislocations.

An overall process of oxide growth and dissolution should result in a decrease of the NPs size, and the surface area seems to be the best integral parameter to monitor this value. Indeed, growth of the oxidation temperature resulted in a gradual increase of S_{BET} for the HF-treated thermally oxidized

SiC NPs (Table 1). The particle sizes (Table 1) estimated from S_{BET} in assumption of the spherical particle shape indicate progressive contraction of SiC core particles with oxidation temperature. According to all aforementioned, an approach of the SiC NPs thermal oxidation followed by oxide removal looks prospective for the NPs size tuning.

Table 1. Surface areas and calculated particle size of the SiC samples after thermal oxidation and oxide removal

Sample	S_{BET}, $m^2 \cdot g^{-1}$	D, nm
SiC_init	110	17.0
SiC_600_HF	123	15.2
SiC_700_HF	129	14.5
SiC_800_HF	156	12.0
SiC_900_HF	200	9.3

3.2. Chemical transformations on the surface of SiC nanoparticles

Change of the SiC NPs color from black to light brown (and spectral data discussed below) under thermal oxidation at 600 ^{o}C indicates removal of carbon and SiC_{1+x} impurities under this treatment. To minimize their influence, further chemical transformations were performed for the SiC_600 sample. Any samples, derived from this solid, are further referenced to without temperature indication (SiC_HF instead of SiC_600_HF). Characterization of the surface groups was performed mainly by diffuse reflectance FT-IR (DRIFT) spectroscopy, supported by XPS and TPD-MS. All different routes of SiC chemical functionalization discussed below and corresponding sample referencing are presented on the flowchart (Fig. 3). Chemical transformation on this flowchart had a purpose of oxide-free SiC NPs preparation in reductive (SiC_HF) and oxidative (SiC_HF/HNO_3)

conditions, probes of their functionalization with organic groups (SiC-C_{18}, SiC-NHC_9 and SiC-NH_2) and preparation of hydroxylated oxide-free SiC_KOH.

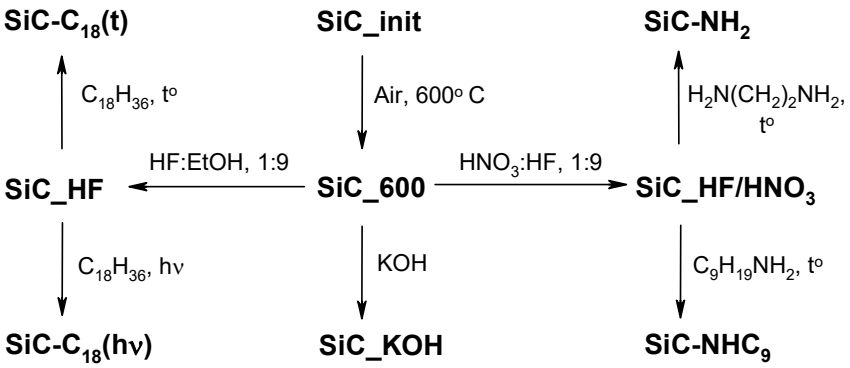

Figure 3. The flowchart of chemical transformations and referencing of functionalized SiC NPs.

DRIFT spectra of the initial, thermally oxidized and oxide-free SiC NPs are shown in Fig. 4. Intense absorption bands of the SiC lattice distorted by reflectance (so-called reststrahlen band [58]) resulted in complete absorbance below 1250 cm^{-1} making the spectra non-informative in this region. Intense bands at 1325, 1540 and 1630 cm^{-1} are due to different combination modes of SiC lattice [59]. Initial SiC sample demonstrates very low IR reflectivity in all studied range, which is typical for carbon containing samples, however wide band (3000 – 3700 cm^{-1}) of OH groups and weak bands of CH_x (2800 – 3000 cm^{-1}), C_3Si–H (2120 cm^{-1}) and C=O (1730 cm^{-1}) fragments could be seen.

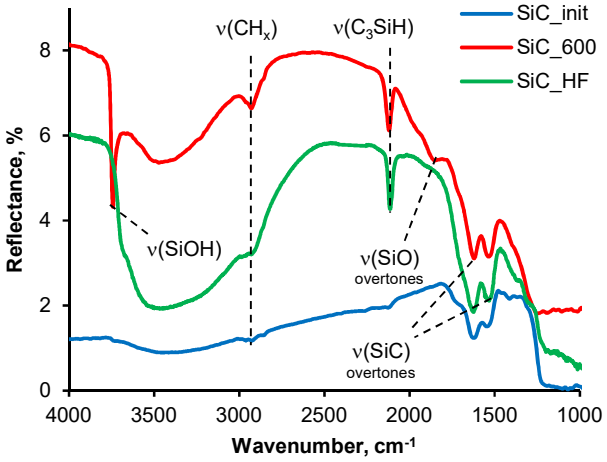

Figure 4. DRIFT spectra of initial SiC_NPs, SiC_600 and SiC_HF. The spectra are stacked.

Thermal treatment at 600°C resulted in a noticeable increase of SiC NPs IR reflectivity, probably due to carbon burning off (see also Raman data, Fig. S1, SI). Intense bands of the silanol groups (3750 cm^{-1} – isolated silanols, wide band at 3000 – 3700 cm^{-1} – H-bonded hydroxyls) and SiO_2 (combination mode of SiO_2 at 1870 cm^{-1}; see also transmittance spectra in Fig. 2) indicate the presence of hydroxylated silica layer on the SiC_600 surface. Surprisingly, the bands of CH_x (2800 – 3000 cm^{-1}) and C_3Si–H (2120 cm^{-1}) groups are clearly seen in the spectrum of thermally oxidized sample. Appearance of these groups is caused by reaction between H_2O (which is present in ambient atmosphere) and strained Si–C bonds on the interface between the SiC and surface oxide layer.

Treatment of oxidized SiC with HF resulted in the disappearance of SiO_2 (1080, 1230 and 1870 cm^{-1}) and isolated silanol (3750 cm^{-1}) bands due to oxide layer removal. However, different from well-known reaction of oxidized silicon with HF, the surface of SiC_HF remains highly hydroxylated, as the band H-bonded hydroxyls significantly increases in its' spectrum in comparison with SiC_600. This result is in line with the earlier findings for monocrystalline SiC wafers [26]. As for CH_x and C_3Si–H bands, removal of oxide layer seems to have no action on them except slight intensity increase and wavenumber shift (2115 cm^{-1}) for the C_3Si–H band.

More detailed information on the chemistry of the initial, thermally oxidized and oxide-free SiC NPs could be extracted from XPS data. Elemental composition of the samples is presented in Table 2. Changes of the Si/C ratio within the sample indicate oxidation of carbon and SiC surface layers in the SiC_600 and consecutive oxide removal in the SiC_HF. Significant fraction of oxygen in the SiC_init and SiC_600 is due to the presence of oxide layer, while for the SiC_HF it relates to surface hydroxyls. Presence of fluorine in the HF-treated sample clearly indicates appearance of fluorinated surface species.

Deconvolutions of the C 1s, Si 2p, O 1s and F 1s core level XPS spectra are presented in Fig. 5. The initial SiC NPs demonstrate C 1s peaks positioned at 282.5 eV (SiC), 284.1 eV (Carbon and Si_3C–O surface fragments), 285.3 (carbon atoms neighboring the C–O species) and 286.8 eV (C_3C–O

fragments). The Si 2p spectrum deconvoluted into peaks at 100.4, 102.2 and 103.4 eV, corresponding to the SiC, silicon oxocarbide (C_2SiO_2 fragments) and SiO_2 species respectively. The main component in the O 1s spectrum at 532.3 eV corresponds to Si–O–Si fragments in SiO_2 and silicon oxocarbide, while other components relate to C–O fragments (533.9 eV) an adsorbed H_2O (536 eV).

Table 2. Elemental composition from the XPS data.

Sample	Atomic %			
	C	Si	O	F
SiC_init	39.6	36.8	23.6	-
SiC_600	20.8	37.7	41.5	-
SiC_HF	39.4	44.3	15.0	1.2

Standard RSF values were used

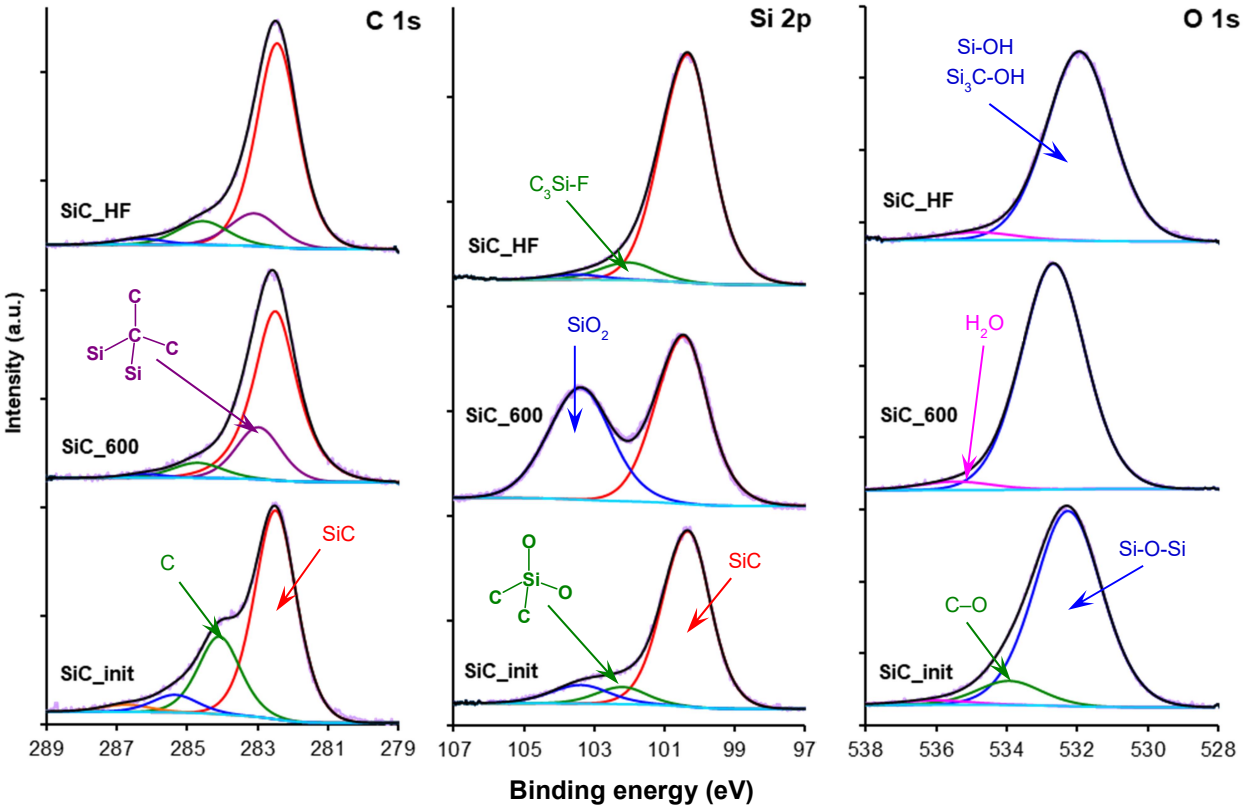

Figure 5. Deconvolutions of XPS spectra. The spectra of different samples are stacked, the intensities are normalized.

Thermal oxidation at 600 ^{o}C resulted in drastic changes in XPS spectra. The C 1s spectrum can be deconvoluted into the main components at 282.5 eV (SiC) and 283.0 eV, which can be related to sub-interfacial strained layers of the SiC as well as to C atoms in C_xCSi_{4-x} coordination. The peaks at 284.7 (Carbon + Si_3C–O) and 286.2 eV (C_3C–O fragments) are rather weak. The Si 2p spectrum can be perfectly (RSTD = 1.03) deconvoluted into two components at 100.6 (FWHM = 1.55) and 103.5 (FWHM = 1.96) eV which can unambiguously be related to SiC and SiO_2. In contrast to the numerous literature data, no silicon oxocarbide peaks were needed to deconvolute the spectrum. The components of the O 1s spectrum correspond to SiO_2 (532.7 eV) and adsorbed H_2O (535.5 eV).

Treatment of oxidized sample with HF does not affect significantly the C 1s spectrum, which can be deconvoluted into the peaks at 282.5 (SiC), 283.1 (sub-interfacial strained SiC + C_xCSi_{4-x}), 284.6 (Carbon + Si_3C–O) and 286.3 (C_3C–O fragments). The only difference between the C 1s spectra of the oxidized SiC NPs before and after the HF treatment is the relative intensities of the 283 and 284.6 eV components. Probably, the oxide removal resulted in some surface relaxation as well as formation of interfacial Si_3C–OH groups, described in [26]. The Si 2p spectrum of the HF-treated sample demonstrates the components at 100.4 eV (SiC), 102.1 eV (C_3Si–OH and C_3Si–F surface groups) and 103.5 eV (residual SiO_2). The O 1s spectrum deconvolutes into 531.9 eV (surface hydroxyls) and 534.8 eV (H_2O) components. Unique peak at 686.3 eV in the F 1s spectrum of SiC_HF (Fig. S4, SI) relates rather to ≡Si–F than ≡C–F species.

According to the DRIFT and XPS data, chemical processes on the SiC surface under thermal oxidation and oxide removal could be described as follows. The oxidation resulted in removal of large fraction of carbon and other impurities and formation of thin (1-2 nm) SiO_2 layer on the SiC surface. In contrast to numerous literature data, no intermediate “silicon oxocarbide” layer was found between SiO_2 and SiC. As the crystalline lattice of SiC mismatches the oxide structure, formed by [SiO_4] tetrahedra, the interface between the SiO_2 and SiC contains a lot of defects and strained bonds. As the oxide layer is permeable to H_2O molecules present in ambient air, these defects readily react

with H_2O forming C_3SiH and CH_x fragments (Fig. 6). Removal of the oxide layer by HF treatment resulted in the surface, covered with H-bonded hydroxyls (≡C–OH or ≡Si–OH depending on crystallographic orientation), C_3Si–H, Si–F and CH_x fragments (see Fig. 6). The presence of strained ≡C–C≡, ≡Si–C≡ and ≡Si–Si≡ bonds as well as sterically-stabilized dangling bonds, similar to ones on reconstructed or hydrogenated SiC surfaces [30, 31], also seems likely.

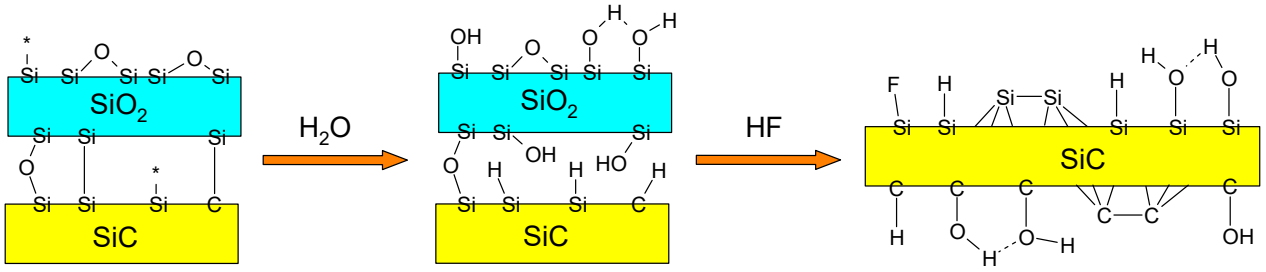

Figure 6. Formation of SiH groups in oxidized SiC and surface species of SiC after oxide removal.

Activity of hydroxylated SiC surfaces towards alkenes [27, 28, 29] as well as presence of C_3Si–H groups potentially active in hydrosilylation, makes alkenes promising for the modification of oxide-free SiC NPs. Indeed, covalent grafting of octadecene on the surface of SiC NPs under both, thermal and photochemical activation can be confirmed by the FTIR spectra (Fig. 7A) demonstrating intense bands of alkyl groups ($\nu_s(CH_2)$ at 2853 cm^{-1}, $\nu_{as}(CH_2)$ at 2925 cm^{-1}, $\nu_{as}(CH_3)$ at 2962 cm^{-1} and $\delta(CH_2)$ at 1462 cm^{-1}) and absence of characteristic alkene band (ν(C=C), 1645 cm^{-1}) inherent for physisorbed $C_{18}H_{36}$. Additional evidence of alkenes covalent grafting is high temperature of SiC-C_{18} thermal decomposition and presence of only short alkenes (C_2 – C_7) among the decomposition products monitored by the TPD-MS method (Fig. 7B). The intensity of ν(Si–H) IR band at 2115 cm^{-1} after grafting of octadecene remains practically unchanged, indicating inactivity of the C_3Si–H groups on the SiC surface in hydrosilylation reaction upon applied conditions. However, detailed nature of alkenes reaction remains unresolved. It can be either formation of ethers with hydroxyls (see Refs. [27, 28, 29]) or addition of the alkenes via the strained bonds (Fig. 8) depending on crystallographic orientation of the surface.

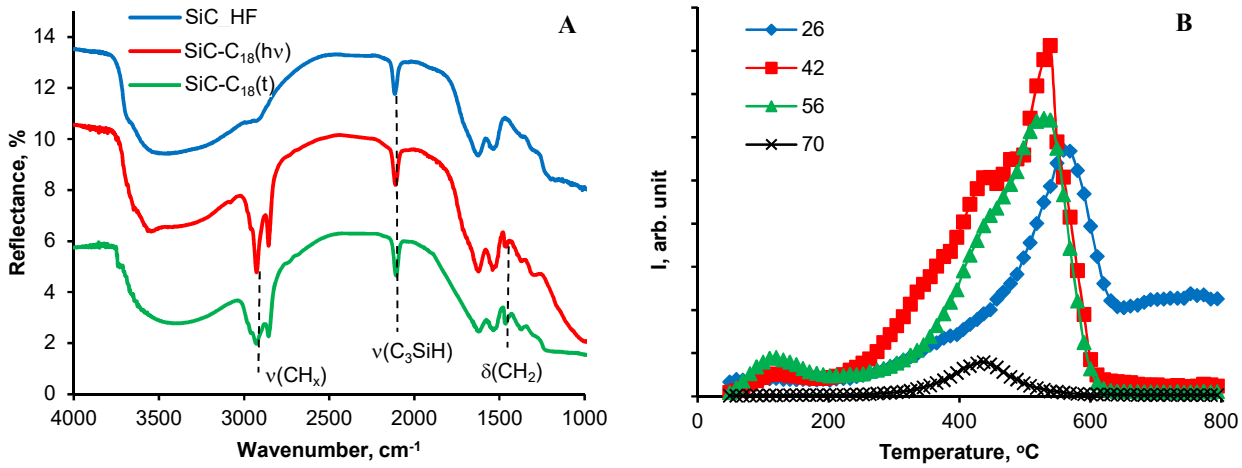

Figure 7. A. DRIFT spectra of SiC_600_HF and products of its modification with 1-octadecene under thermal and photochemical activation. 2. TPD-MS profiles for SiC-C_{18}(t) sample (ions with *m/z* 26 ($C_2H_2^+$), 42 ($C_3H_6^+$), 56 ($C_4H_8^+$) and 70 ($C_5H_{10}^+$)).

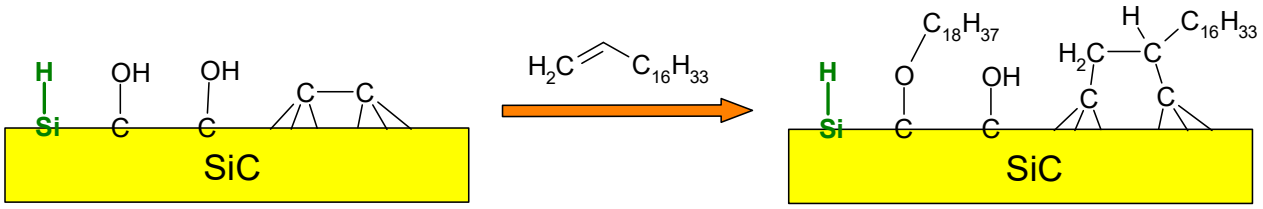

Figure 8. Possible ways of alkenes grafting on the oxide-free SiC.

Apart from the use of HF, the surface of SiC NPs could also be freed from the oxide layer under treatment with KOH solution or with HF/HNO_3 mixture (see transmittance FT-IR spectra in Fig. S5, SI). Surprisingly, the C_3Si–H groups of the SiC surface seem at least partially stable under continuous KOH treatment (Fig. 9) and even after action of aqueous bromine solution. This fact could be explained by their sterical hindrance, similarly as it was shown for dangling bonds on hydrogenated SiC surfaces [30, 31]. Differently from HF-treated SiC, the SiC_KOH contain some hydroxyls (probably, silanols) without H-bonding; their narrow IR band lays at 3700 cm^{-1}, i.e. 50 cm^{-1} towards low wavelengths as compared to SiO_2 layer.

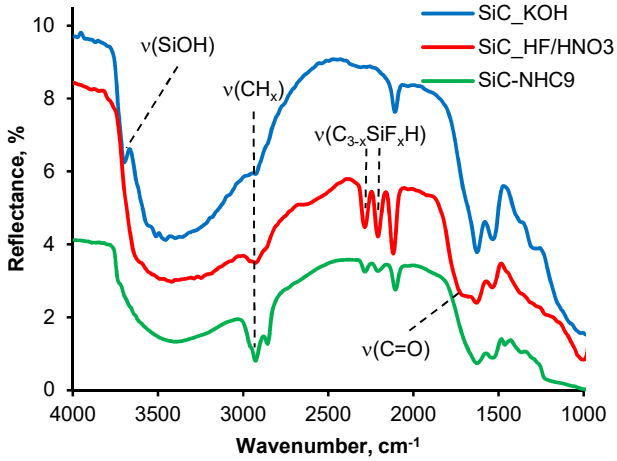

Figure 9. DRIFT spectra of SiC_KOH, SiC_HF/HNO_3 and SiC-NHC_9.

Treatment in HF/HNO_3 mixture was performed in the conditions, close to ones of the "chemical top-down" SiC NPs preparation [33, 34, 35, 36, 37], to achieve similar surface functionalization. First of all, formation of the "carbon fluorooxide" under the etching discussed in details in our recent work [43] should be mentioned. However, scrupulous rinsing of the SiC_HF/HNO_3 sample after the reaction ensures its' purification from any CFO, which is well-soluble under these conditions. According to the DRIFT data, the surface chemistry of SiC_HF/HNO_3 demonstrates a number of differences from the SiC_HF. The surface of SiC_HF/HNO_3 bears significant fraction of carboxylic acid groups (ν(C=O), shoulder at 1730 cm^{-1}), higher fraction of CH_x groups (increase of the band ν(CH_x) at 2800 – 3000 cm^{-1}) and two new types of Si–H groups, probably C_2SiFH and $CSiF_2H$ ((ν(SiH) at 2208 and 2287 cm^{-1}). The carboxylic acid groups react with $C_9H_{19}NH_2$ forming amides, which can be monitored by appearance of intense bands of the alkyl group and disappearance of ν(C=O) band at 1730 cm^{-1} due to coincidence between the amide ν(C=O) (approx. 1670 cm^{-1}) and SiC combination mode.

Different from the SiC_HF and similarly to electrochemically-derived porous SiC [42], the surface of SiC_HF/HNO_3 bears a layer enriched in carbon (see Raman data, Fig. S1, SI).

The quantification of SiC NPs surface layers was performed by thermal analysis (Fig. 10A) and pH-titration (Fig. 10B). The mass loss below 150°C on the TG curve is attributed to desorption of physisorbed water, that is why the starting mass of the sample was set as actual value at this temperature. The mass loss between 200 and 500°C accompanied by exothermic effect on the DTA relates to oxidation of grafted organic groups, while the mass gain up to 1150°C corresponds to transformation of SiC into SiO_2. Increase of the temperature above 950°C gives sharp exothermic effect on the DTA curve indicating fast oxidation of the SiC due to the increase of SiO_2 surface shell permeability to O_2 at this temperature range. The mass value above 1150°C is nearly constant confirming complete transformation of all studied solids into SiO_2 and volatile products.

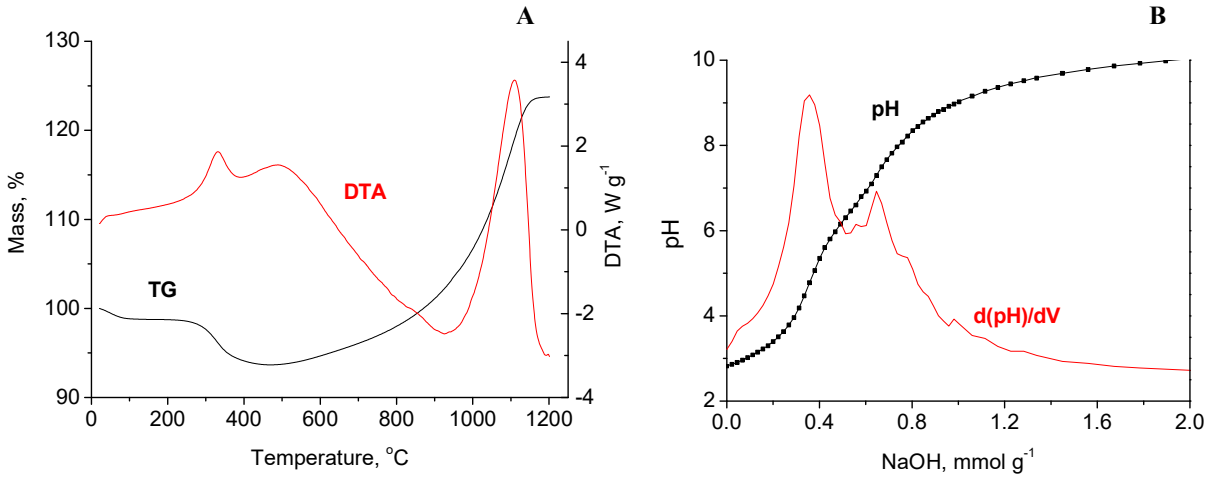

Figure 10. A. TG and DTA curves of SiC-C_{18}(t) sample. B. pH-titration curve for SiC_HF/HNO_3.

To perform calculations, all "non-SiC" part of the sample SiC_600 was assumed as an oxide (SiO_2), while for all other samples the presence of oxide was neglected and all "non-SiC" components (carbon, hydroxyls, organic groups) were assumed as those, burning totally below 1200°C without any solid residue. The results of quantitative analysis are presented in Table 3.

Fraction of SiC in SiC_600 NPs allowed estimation of SiO_2 layer thickness as 0.63 nm. This small value, corresponding to just few layers of [SiO_4] tetrahedra, explains the reactivity of SiC/SiO_2 interface towards H_2O vapor under ambient conditions. Low fraction of "non-SiC" in SiC_HF sample

allowed relation of all surface groups to one surface monolayer, while for the SiC_HF/HNO_3 approximately 1 nm thick carbon-enriched layer is formed. High concentrations of grafted alkyl groups in SiC_C_{18}(t) and SiC_NHC_9 samples (for –$C_{18}H_{37}$ its value corresponds to formation of disordered monolayer) confirm high efficiency of proposed functionalization methods.

Table 3. Quantitative composition of modified SiC NPs.

Sample	W(SiC), %	Surface groups	W(%)	C_L, μmol g^{-1}
SiC_init	86.2	Carbon	13.8	-
SiC_600	84.3	SiO_2	15.7	-
SiC_HF	95.1	CH_x, –OH	4.9	-
SiC_C_{18}(t)	83.6	CH_x, –OH	4.4	-
		–$C_{18}H_{37}$	12.0	478
SiC_HF/HNO_3	87.8	Carbon, CH_x, –OH	12.2	-
		–CO_2H	-	354*
		≡Si–OH	-	295*
SiC_NHC_9	85.2	Carbon, CH_x, –OH	10.7	-
		–$CONHC_9H_{19}$	4.1	240

*Data from pH-titration, see below. C_L is the concentration of functional groups. Taking into account all the assumptions made, the relative uncertainty for C_L values are estimated to be in the range of 10-20 %.

The concentrations of acidic surface groups in SiC_HF/HNO_3 were determined by pH-potentiometric titration method. Two inflections corresponding to –CO_2H and ≡Si-OH groups with pK_a equal to 3.35 and 6.23 can be seen on the titration curve (Fig. 10B). Values of pK_a are slightly lower in comparison with reported data by Beke *et al.* [41], while the groups ≡C-OH were not

detected due to their low acidity (pK_a ~ 10) and incomplete deprotonation under our experiment conditions.

Hydrophilic surface of SiC_KOH, SiC_HF/HNO_3 and SiC_NH_2 samples makes them suitable for preparation of aqueous sols, which can be made without any special dispersion techniques such as colloidal milling or application of high power ultrasound. Figure 11 shows the results of sols characterization by dynamic light scattering method.

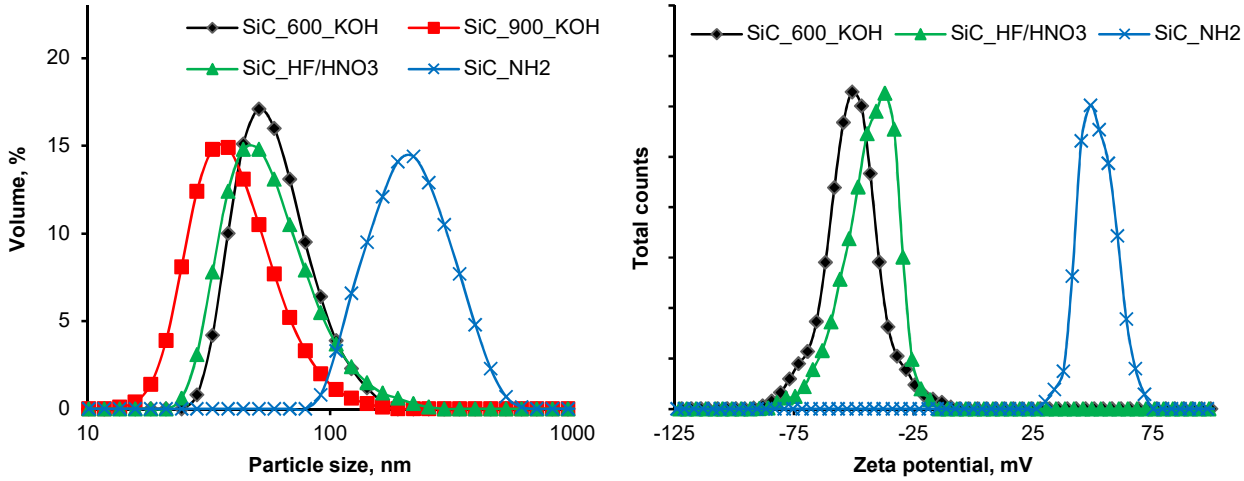

Figure 11. Particle size distributions and zeta potentials of chemically modified SiC NPs.

Table 4. Characteristics of SiC NPs sols.

Sample	Particle size, nm	Zeta potential, mV
SiC_600_KOH	50	-51
SiC_900_KOH	35	-51
SiC_HF/HNO_3	45	-37
SiC_NH_2	215	+49

Zeta-potentials of studied NPs (Table 4) are stipulated by the chemical nature of their surface groups, existing as anions (≡Si–O^- and –CO_2^-) or cations (–$CH_2CH_2NH_3^+$) in aqueous solution.

Slightly smaller potential for the SiC_HF/HNO_3 in comparison with the SiC_KOH NPs is caused by residues of electrolyte (acid for SiC_HF/HNO_3 and alkali for SiC_KOH) used for sols preparation.

For all studied sols the DLS particle sizes are in the nanometers range without any large aggregates (Table 4). However they are significantly larger in comparison with TEM and N_2-adsorption data. This difference could be explained by the presence of aggregates formed by a few tightly-fused SiC NPs, with a surface area close to the sum of ones for separated NPs. Decrease of the particle size due to the growth of the oxidation temperature (see Table 1) causes the same effect on the DLS size value. Slightly smaller size of SiC_HF/HNO_3 as compared with the SiC_600_KOH could take place due to partial SiC dissolution in HF/HNO_3 solution. The size of SiC_NH_2 increases significantly in comparison with SiC_HF/HNO_3 particles, used for their preparation. Probably this change takes place due to cross-linking of the SiC NPs by bifunctional ethylenediamine molecules used for functionalization, and significant improvement of synthesis conditions is needed to avoid cross-linking.

5. Conclusions

In this paper we presented some new insights into SiC chemical behavior. Particularly, we demonstrated that thermal oxidation of highly-dispersed 3C-SiC resulted in formation of a thin hydroxylated SiO_2 layer on its' surface, while an appearance of "silicon oxocarbide" in studied conditions seems doubtful. The process of controllable thermal oxidation followed by oxide removal was successfully applied for the SiC NPs size tuning. The permeability of thin disordered SiO_2 layers to oxygen and water molecules as well as a mismatch of the SiC and SiO_2 lattice parameters induce formation of C_3Si–H and CH_x fragments onto the SiO_2/SiC interface under ambient conditions.

Removal of oxide layers either by HF or KOH treatments resulted in SiC NPs, covered mainly by hydroxyl and C_3Si–H groups. The surface of oxide-free SiC NPs could be efficiently modified by thermally or photochemically initiated reaction with alkenes. This reaction does not proceed as

hydrosilylation of C_3Si–H groups. However, its exact nature, i.e., interaction of alkene molecules with hydroxyls or/and with strained surface Si–Si or C–C bonds remains under discussion. Treatment of thermally oxidized SiC NPs with a HF/HNO_3 mixture produces two products: SiC NPs with carbon-enriched surface layer bearing carboxylic acid groups and soluble carbon fluorooxide. The latter is similar to that forming under SiC anodic etching. Further functionalization of carboxylated SiC surface could be readily achieved via amide chemistry. Highly hydrophilic SiC particles, such as hydroxylated (SiC_KOH), carboxylated (SiC_HF/HNO_3) or aminated (SiC_NH_2) form aqueous sols, stable under storage in close vessels for at least 1 year.

Supporting Information Available

Raman spectra, nitrogen adsorption isotherm, diffuse reflectance UV-vis spectra, F 1s XPS spectrum, transmittance FTIR spectra (KBr pellets) of studied SiC NPs, and corresponding brief descriptions. This material is available free of charge via the Internet at "http://pubs.acs.org".

Acknowledgments

The authors are grateful to Dr. Galina Dovbeshko from Institute of Physics of NAS of Ukraine (Kyiv) for Raman measurements, Dr. Igor Zatovskiy and Dr. Oleksandr Bieda from Taras Shevchenko National University of Kyiv for TGA, XRD and TPD-MS measurements, Dr. Roland Barbosa from Universite Libre de Bruxelles (Belgium) for XPS measurements and Mr. Peter Stone from Aston University (UK) for helpful discussion. This work was supported by EU FP-7 MSCA-IRSES grant (GA #319013, "Porous Silicon Carbide as a Support for Co Metal Nanoparticles in Fischer-Tropsch Synthesis") and EU Horizon 2020 MSCA-RISE grant (Project 690945 "Carbon-based nano-materials for theranostic application") which are gratefully acknowledged.

References

1. Abderrazak, H.; Bel Hadj Hmida, E.S. Silicon Carbide: Synthesis and Properties. Chapter 16 in *Properties and Applications of Silicon Carbide*.; InTech, **2011**; pp. 361-388.
2. Shackelford, J. F.; Alexander, W. (Eds). *Materials Science and Engineering Handbook* (3rd Ed.), CRC Press LLC, **2001**.
3. Castelletto, S.; Johnson, B. C.; Zachreson, C.; Beke, D.; Balogh, I.; Ohshima, T.; Aharonovich, I.; Gali, A. Room Temperature Quantum Emission from Cubic Silicon Carbide Nanoparticles. *ACS Nano* **2014**, *8(8)*, 7938–7947.
4. Askari, S.; Haq, A. U.; Macias-Montero, M.; Levchenko, I.; Yu, F.; Zhou, W.; Ostrikov, K.; Maguire, P.; Svrcek, V.; Mariotti, D. Ultra-Small Photoluminescent Silicon-Carbide Nanocrystals by Atmospheric-Pressure Plasmas. *Nanoscale* **2016**, *8*, 17141-17149.
5. Round, H. J. A Note on Carborundum. *Electrical World* **1907**, *19*, 309.
6. Paarmanna, A.; Razdolski, I.; Melnikov, A.; Gewinner, S.; Schöllkopf, W.; Wolf, M. Second Harmonic Generation Spectroscopy in the Reststrahl Band of SiC Using an Infrared Free-Electron Laser. *Appl. Phys. Lett.* **2015**, *107*, 081101.
7. Zakharko, Y.; Nychyporuk, T.; Bonacina, L.; Lemiti, M.; Lysenko, V. Plasmon-enhanced nonlinear optical properties of SiC nanoparticles. *Nanotechnology* **2013**, *24*, 055703 (6pp)
8. Alekseev, S. A.; Korytko, D. M.; Gryn, S. V.; Iablokov, V.; Khainakova, O. A.; Garcia-Granda, S.; Kruse, N. Silicon Carbide with Uniformly Sized Spherical Mesopores from Butoxylated Silica Nanoparticles Template. *J. Phys. Chem. C*. **2014**, *118(41)*, 23745–23750.
9. Shcherban, N. D. Review on Synthesis, Structure, Physical and Chemical Properties and Functional Characteristics of Porous Silicon Carbide. *J. Ind. Eng. Chem*. **2017**, *50*, 15–28.
10. Huczko, A.; Bystrzejewski, M.; Lange, H.; Fabianowska, A.; Cudziło, S.; Panas A.; Szala, M. Combustion Synthesis as a Novel Method for Production of 1-D SiC Nanostructures. *J. Phys. Chem. B.* **2005**, *109(34)*, 16244–16251.
11. Zekentes, K; Rogdakis, K. SiC Nanowires: Material and Devices. *J. Phys. D: Appl. Phys*. **2011**, *44*, 133001.
12. Rahaman, M. N. *Ceramic Processing (2nd Ed*); CRC Press, **2017**.
13. Mobargan Bonab, M.A.; Simchi, A. Effect of Silicon Carbide Nanoparticles on Hot Deformation of Ultrafine-Grained Aluminium Nanocomposites Prepared by Hot Powder Extrusion Process. *Powder Metallurgy* **2016**, *59(4)*, 262-270.
14. Naeimirad, M.; Zadhoush, A.; Neisiany, R. E. Fabrication and Characterization of Silicon Carbide/Epoxy Nanocomposite Using Silicon Carbide Nanowhisker and Nanoparticle Reinforcements. *J. Compos. Mater.* **2015**, *50(4)*, 435 – 446.
15. Alizadeh, O.; Khoramishad, H. Effects of Silicon Carbide Nanoparticles and Multi-Walled Carbon Nanotubes on Water Uptake and Resultant Mechanical Properties Degradation of Polymer Nanocomposites Immersed in Hot Water. *Polym. Compos.* **2017**, *38*, DOI: 10.1002/pc.24303
16. Li, J.; Wang, J.; Gao, D.; Li, X.; Miao, S.; Wang, G.; Bao, X. Silicon Carbide Supported Iron Nanoparticles Encapsulated in Nitrogen-Doped Carbon for Oxygen Reduction Reaction. *Catal. Sci. Technol.*, **2016**, *6*, 2949-2954.
17. Liu, H.; She, G.; Mu, L.; Shi, W. Porous SiC Nanowire Arrays as Stable Photocatalyst for Water Splitting Under UV Irradiation. *Mater. Res. Bull.* **2012**, *47(3)*, 917–920.
18. Wang, B.; Wang, Y.; Lei, Y.; Wu, N.; Gou, Y.; Han, C.; Xie, S.; Fang, D. Mesoporous Silicon Carbide Nanofibers with in Situ Embedded Carbon for Co-Catalyst Free Photocatalytic Hydrogen Production. *Nano Res.* **2016**, *9(3)*, 886-898.
19. Jiao, Z.; Zhai, Z.; Guo, X.; Guo, X.-Y. Visible-Light-Driven Photocatalytic Suzuki-Miyaura Coupling Reaction on Mott-Schottky-type Pd/SiC Catalyst. *J. Phys. Chem. C.* **2015**, *119*, 3238−3243.

20. Oliveros, A.; Guiseppi-Elie, A.; Saddow, S. E. Silicon Carbide: a Versatile Material for Biosensor Applications. *Biomed. Microdevices* **2013**, *15*, 353–368.
21. Pourreza, N.; Naghdi, T. Silicon Carbide Nanoparticles as an Adsorbent for Solid Phase Extraction of Lead and Determination by Flame Atomic Absorption Spectrometry. *J. Ind. Eng. Chem*. **2014**, *20(5)*, 3502–3506.
22. Gupta, V. K.; Fakhri, A.; Rashidi, S.; Ibrahim, A. A.; Asif, M.; Agarwal, S. Optimization of Toxic Biological Compound Adsorption from Aqueous Solution onto Silicon and Silicon Carbide Nanoparticles through Response Surface Methodology. *Mater. Sci. Eng. C*. **2017**, *77*, 1128-1134.
23. Fan, J.; Li, H.; Jiang, J.; So, L. K. Y.; Lam, Y. W.; Chu, P. K. 3C–SiC Nanocrystals as Fluorescent Biological Labels. *Small* **2008**, *4*, 1058-1062.
24. Botsoa, J.; Lysenko, V.; Géloën, A.; Marty, O.; Bluet, J.-M.; Guillot, G. Application of 3C-SiC Quantum Dots for Living Cell Imaging. *Appl. Phys. Lett.* **2008**, *92*, 173902 (3 pp).
25. Boksebeld, M.; Kilin, V.; Geloën, A.; Ceccone, G.; Jaffal, A.; Schmidt, C.; Alekseev, S.; Lysenko, V.; Wolf, J. P.; Bonacina, L.; Souteyrand, E.; Chevolot Y.; Monnier, V. Folate-Modified Silicon Carbide Nanoparticles for Cancer Cell Targeting Using Multiphoton Microscopy. *RSC Adv.* **2017**, *7*, 27361-27369.
26. Dhar, S.; Seitz, O.; Halls, M. D.; Choi, S.; Chabal, Y.J.; and Feldman, L. C. Chemical Properties of Oxidized Silicon Carbide Surfaces upon Etching in Hydrofluoric Acid. *J. Am. Chem. Soc*. **2009**, *131*, 16808–16813.
27. Rosso, M.; Arafat, A.; Schroen, K.; Giesbers, M.; Roper, C. S.; Maboudian, R.; Zuilhof, H. Covalent Attachment of Organic Monolayers to Silicon Carbide Surfaces. *Langmuir* **2008**, *24*, 4007-4012.
28. Rosso, M.; Giesbers, M.; Arafat, A.; Schroen, K.; Zuilhof, H. Covalently Attached Organic Monolayers on SiC and Si_xN_4 Surfaces: Formation Using UV Light at Room Temperature. *Langmuir* **2009**, *25*, 2172-2180.
29. Steenackers, M.; Sharp, I. D.; Larsson, K.; Hutter, N.A.; Stutzmann, M.; Jordan, R. Structured Polymer Brushes on Silicon Carbide. *Chem. Mater.* **2010**, *22*, 272–278.
30. Derycke, V.; Soukiassian, P.G.; Amy, F.; Chabal, Y. J.; D'angelo, M. D.; Enriquez, H. B.; Silly, M. G. Nanochemistry at the Atomic Scale Revealed in Hydrogen-Induced Semiconductor Surface Metallization. *Nat. Mater.* **2003**, *2(4)*, 253-258.
31. Soukiassian, P. Engineering Cubic Silicon Carbide Surfaces Properties Using Hydrogen: Metallization versus Passivation. *Appl. Phys. A.* **2006**, *82*, 421–430.
32. Forbeaux, I.; Themlin, J.-M.; Debever, J.-M. Heteroepitaxial Graphite on 6H-SiC (0001): Interface Formation Through Conduction-Band Electronic Structure. *Phys. Rev. B.* **1998**, *58*, 16396-16406.
33. Zhu, J.; Liu, Z.; Wu, X. L.; Xu, L. L.; Zhang, W. C.; Chu., P. K. Luminescent Small-Diameter 3C-SiC Nanocrystals Fabricated via a Simple Chemical Etching Method. *Nanotechnology* **2007**, *18*, 365603 (5 pp).
34. Wu, X. L.; Xiong, S. J.; Zhu, J.; Wang, J.; Shen, J. C.; Chu., P. K. Identification of Surface Structures on 3C-SiC Nanocrystals with Hydrogen and Hydroxyl Bonding by Photoluminescence. *Nano. Lett.* **2009**, *9*, 4053-4060.
35. Beke, D.; Szekre´nyes, Z.; Balogh, I.; Veres, M.; Fazakas, E.; Varga, L. K.; Kamara´s, K.; Cziga´ny, Z.; Gali, A. Characterization of Luminescent Silicon Carbide Nanocrystals Prepared by Reactive Bonding and Subsequent Wet Chemical Etching. *Appl. Phys. Lett.* **2011**, 99, 213108 (3 pp).
36. Beke, D.; Szekrenyes, Z.; Balogh, I.; Czigany, Z.; Kamaras, K.; Gali, A. Preparation of Small Silicon Carbide Quantum Dots by Wet Chemical Etching. *J. Mater. Res.* **2013**, *28(1)*, 44-49.
37. Li, Y.; Chen, C.; Li J.-T.; Yang, Y.; Lin, Z.-M. Surface Charges and Optical Characteristic of Colloidal Cubic SiC Nanocrystals. *Nanoscale Res. Lett.* **2011**, *6*, 454 (7 pp).

38. Fan, J.Y.; Li, H.X.; Zhang, N.; Lu, R.F. Identification of the Reconstruction and Bonding Structure of SiC Nanocrystal Surface by Infrared Spectroscopy. *Appl. Surf. Sci.* **2011**, *258*, 627-630.
39. Zakharko, Y.; Botsoa, J.; Alekseev, S.; Lysenko, V.; Bluet, J.-M.; Marty, O.; Skryshevsky, V.A.; Guillot, G. Influence of the Interfacial Chemical Environment on the Luminescence of 3C-SiC Nanoparticles. *J. Appl. Phys.* **2010**, *107*, 013503 (7 pp).
40. Mwania, M.; Janáky, C.; Rajeshwar, K.; Kroll, P. Fabrication of β-SiC Quantum Dots by Photo-Assisted Electrochemical Corrosion of Bulk Powders. *Electrochem. Commun.* **2013**, *37*, 1-4.
41. Beke, D.; Jánosi, T. Z .; Somogyi, B.; Major, D. Á.; Szekrényes, Z.; Erostyák, J.; Kamarás, K.; Gali, A. Identification of Luminescence Centers in Molecular-Sized Silicon Carbide Nanocrystals. *J. Phys. Chem. C*. **2016**, *120*, 685−691.
42. Alekseev, S.A.; Zaitsev, V. N.; Botsoa, J.; Barbier, D. Fourier Transform Infrared Spectroscopy and Temperature-Programmed Desorption Mass Spectrometry Study of Surface Chemistry of Porous 6H-SiC. *Chem. Mater.* **2007**, *19*, 2189-2194.
43. Alekseev, S.; Korytko, D.; Iazykov, M.; Khainakov, S.; Lysenko, V. Electrochemical Synthesis of Carbon Fluorooxide Nanoparticles from 3C-SiC Substrates. *J. Phys. Chem. C.* **2015***, 119(35)*, 20503–20514.
44. Tishchenko, I.Y.; Ilchenko, O.O.; Kuzema, P.O. TGA-DSC-MS Analysis of Silicon Carbide and of Its Carbon-Silica Precursor. *Chem. Phys. Technol. Surf.* **2015**, *6(2)*, 216-223.
45. Vennekamp, M.; Bauer, I.; Groh, M.; Sperling, E.; Ueberlein, S.; Myndyk, M.; Mäder , G.; Kaskel, S. Formation of SiC nanoparticles in an atmospheric microwave plasma. *Beilstein J. Nanotechnol*. **2011**, *2*, 665–673.
46. Shimoda, K.; Park, J.-S.; Hinoki, T.; Kohyama, A. Influence of Surface Structure of SiC Nano-Sized Powder Analyzed by X-ray Photoelectron Spectroscopy on Basic Powder Characteristics. *Appl. Surf. Sci.* **2007**, *253,* 9450-9456.
47. Yakimova, R.; Petoral Jr, R. M.; Yazdi, G. R.; Vahlberg, C.; Lloyd Spetz, A.; Uvdal, K. Surface Functionalization and Biomedical Applications Based on SiC. *J. Phys. D: Appl. Phys*. **2007**, *40*, 6435–6442.
48. Petoral, Jr., R. M.; Yazdi, G. R.; Lloyd Spetz, A.; Yakimova, R.; Uvdal, K. Organosilane-Functionalized Wide Band Gap Semiconductor Surfaces. *Appl. Phys. Lett*. **2007**, *90*, 223904 (3 pp).
49. Luo, Y.; Rong, M. Z.; Zhang, M. Q.; Friedrich, K.S.; Surface Grafting onto SiC Nanoparticles with Glycidyl Methacrylate in Emulsion. *J. Polym. Sci. A*. **2004**, *2*, 3842-3852.
50. Rong, M. Z.; Zhang, M. Q.; Shi, G.; Ji, Q. L.; Wetzel, B.; Friedrich, K. Graft Polymerization onto Inorganic Nanoparticles and Its Effect on Tribological Performance Improvement of Polymer Composites. *Tribol. Int*. **2003**, *36*, 697–707.
51. Yegorov, A. S.; Ivanov, V. S.; Antipov, A.V.; Wozniak, A. I.; Tcarkova, K.V. Chemical Modification Methods of Nanoparticles of Silicon Carbide Surface (Review). *Oriental J. Chem.* **2003**, *36*, 697–707.
52. Nomura, Y.; Iijima, M.; Kamiya, H. Hydrophobic Group Functionalization of Polyethyleneimine for Controlling Dispersion Behavior of Silicon Carbide Nanoparticles in Aqueous Suspension. *J. Am. Ceram. Soc*. **2012**, *95(11)*, 1–7.
53. Loganathan, S.; Sankaran, S. Surface Chemical Studies on Silicon Carbide Suspensions in the Presence of Poly (Ethylene Glycol) and Chitosan. *Colloid and Surface Science*. **2017**, *2(1)*, 6-20.
54. Iijima, M.; Kamiya, H. Surface Modification of Silicon Carbide Nanoparticles by Azo Radical Initiators. *J. Phys. Chem. C.* **2008**, *112*, 11786–11790.
55. Szekrényes, Z.; Somogyi, B.; Beke, D.; Károlyházy, G.; Balogh, I.; Kamarás, K.; Gali, A. Chemical Transformation of Carboxyl Groups on the Surface of Silicon Carbide Quantum Dots. *J. Phys. Chem. C.* **2014**, *118*, 19995−20001.
56. Jenkins, R.; Snyder, R.L. *Introduction to X-ray Powder Diffractometry*, John Wiley & Sons Inc., **1996**.

57. Alekseev, S. A.; Zaitsev, V. N.; Fraissard, J. Organosilicas with Covalently Bonded Groups under Thermochemical Treatment. *Chem. Mater*. **2006**, *18(7)*, 1981.
58. MacMillan, M. F.; Devaty, R. P.; Choyke, W. J.; Goldstein, D. R.; Spanier, J. E.; Kurtz, A. D. Infrared Reflectance of Thick p-type Porous SiC Layers. *J. Appl. Phys.* **1996**, *80(4)*, 2412 - 2419.
59. Hofmeister, A. M.; Pitman, K. M.; Goncharov, A. F.; Speck, A. K. Optical Constants of Silicon Carbide for Astrophysical Applications. II. Extending Optical Functions from Infrared to Ultraviolet Using Single-Crystal Absorption Spectra. *Astrophys. J.* **2009**, *696*, 1502–1516.